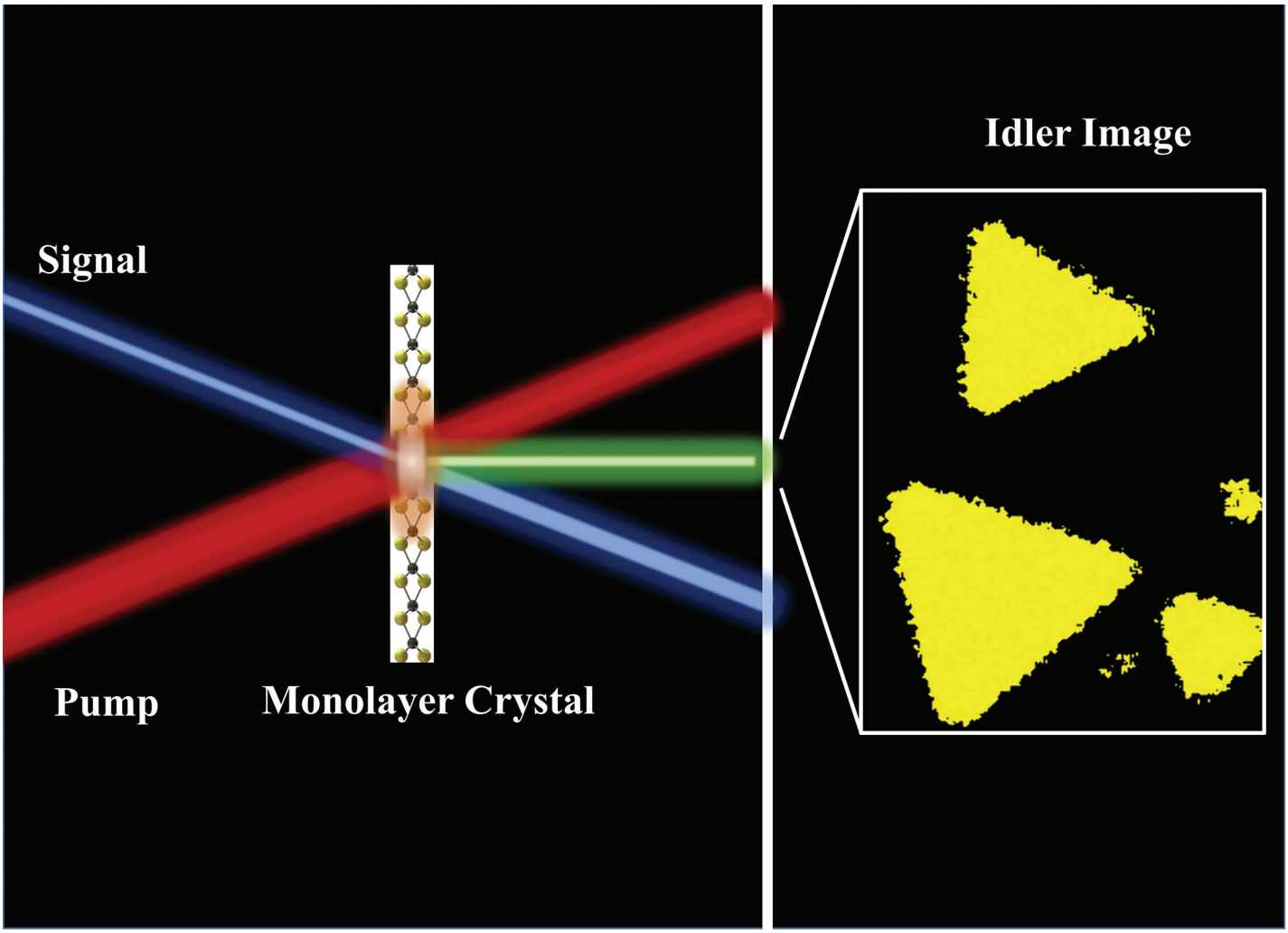

Showcasing research from Collaboration of Professor Zhipei Sun's laboratory, Department of Electronics and Nanoengineering, Aalto University, Espoo, Finland; and Professor Jianlin Zhao's laboratory, Shaanxi Key Laboratory of Optical Information Technology, Northwestern Polytechnical University, Xi'an, China.

Difference Frequency Generation in Monolayer MoS_2

Difference frequency generation (DFG) plays an important role in coherent emission for numerous applications, ranging from sensing and imaging. Here, for the first time, we demonstrate DFG in two-dimensional layered semiconductors. Such a highly efficient, broadband, phase-matching-free down-conversion nonlinear optical process in two-dimensional layered materials, may open new ways to their nonlinear optical applications, such as coherent light generation and parametric amplification.

As featured in:

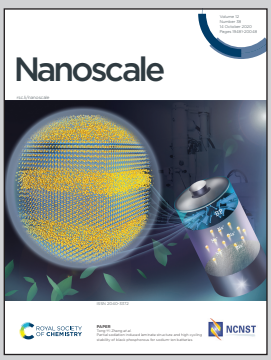

See Masood Ghotbi, Jianlin Zhao, Zhipei Sun *et al.*, *Nanoscale*, 2020, **12**, 19638.

ROYAL SOCIETY OF CHEMISTRY

rsc.li/nanoscale

Registered charity number: 207890

Nanoscale

ROYAL SOCIETY OF CHEMISTRY

PAPER

View Article Online
View Journal | View Issue

Cite this: *Nanoscale*, 2020, **12**, 19638

Difference frequency generation in monolayer MoS_2

Yadong Wang, [a,b] Masood Ghotbi, *[c] Susobhan Das, [b] Yunyun Dai, [b] Shisheng Li, [d] Xuerong Hu, [b,e] Xuetao Gan, [a] Jianlin Zhao *[a] and Zhipei Sun *[b]

Received 10th March 2020,
Accepted 28th May 2020

DOI: 10.1039/d0nr01994a

rsc.li/nanoscale

Difference frequency generation has long been employed for numerous applications, such as coherent light generation, sensing and imaging. Here, we demonstrate difference frequency generation down to atomic thickness in monolayer molybdenum disulfide. By mixing femtosecond optical pulses at wavelength of 406 nm with tunable pulses in the spectral range of 1300–1520 nm, we generate tunable pulses across the spectral range of 550–590 nm with frequency conversion efficiency up to ~2×10^{-4}. The second-order nonlinear optical susceptibility of monolayer molybdenum disulfide, $\chi^{(2)}_{\text{eff}}$, is calculated as ~1.8×10^{-8} m V^{-1}, comparable to the previous results demonstrated with second harmonic generation. Such a highly efficient down-conversion nonlinear optical process in two-dimensional layered materials may open new ways to their nonlinear optical applications, such as coherent light generation and amplification.

Introduction

Nonlinear optics, in particular nonlinear frequency conversions, have significantly expanded the applications of the lasers in many fields.[1,2] Widely tunable laser systems in different spectral ranges are provided by nonlinear frequency conversion schemes using second- and third-order nonlinear optical processes. Among the second-order nonlinear optical processes, difference frequency generation (DFG), as a building block for a large range of applications, is of great significance. It plays the main role for generating coherent light at longer wavelengths and acts as the base for other second-order nonlinear parametric interactions such as optical parametric generation (OPG), amplification (OPA) and oscillation (OPO),[1,2] which enable to produce tunable light sources across different spectral regions for a large variety of applications including material characterizations,[3] laser spectroscopy,[4] and molecular sensing.[5]

Currently, there are major obstacles in scaling down the nonlinear frequency conversion systems to micro- and nanoscale regimes for various emerging applications, mainly due to the relatively low optical nonlinearity coefficients of the traditional bulk nonlinear optical materials. Introducing the two-dimensional (2D) layered materials with extraordinarily strong nonlinear optical responses for frequency conversions, has created new possibilities for potential on-chip applications.[6,7] For example, monolayer transition-metal dichalcogenides (TMDs) have been demonstrated with strong second-, third- and high-order nonlinearities.[8–12]

Among the second-order frequency conversion nonlinear interactions, second harmonic generation (SHG) and sum frequency generation (SFG) are the common processes that generate light with wavelengths shorter than that of input beams (*i.e.*, up-conversion interactions). Because of its simple implementation, by applying only one input light component as the fundamental beam, SHG has been performed widely in different 2D materials including MoS_2,[11–16] $MoSe_2$,[17,18] WS_2,[19,20] WSe_2,[21] and $MoTe_2$.[22] Similarly, SFG in TMDs has also been reported in recent years.[23–25]

In contrast to the SHG and SFG processes, DFG is a frequency down-conversion second-order nonlinear interaction, thus extending the application range of nonlinear processes to various fields. The exploration of such a process in nanoscale is highly important,[26] especially in 2D materials. Thus far, DFG in graphene has been observed in terahertz region.[27,28] For example, with assistance of graphene plasmon, the photon efficiency of DFG can be as high as 10^{-5} under specific in-plane phase-matching conditions.[28]

[a]*MOE Key Laboratory of Material Physics and Chemistry under Extraordinary Conditions, and Shaanxi Key Laboratory of Optical Information Technology, School of Physical Science and Technology, Northwestern Polytechnical University, Xi'an 710129, China. E-mail: jlzhao@nwpu.edu.cn*
[b]*Department of Electronics and Nanoengineering, Aalto University, Fi-00076 Aalto, Finland. E-mail: zhipei.sun@aalto.fi*
[c]*Department of Physics, University of Kurdistan, P.O. Box 66177-15175, Sanandaj, Iran. E-mail: m.ghotbi@uok.ac.ir*
[d]*International Center for Young Scientists (ICYS), National Institute for Materials Science (NIMS), Tsukuba, Japan*
[e]*Institute of Photonics and Photon Technology, Northwest University, Xi'an 710069, China*

Here, we report the DFG by using monolayer MoS_2 to produce tunable femtosecond pulses in the visible spectral range of 550–590 nm. Such a nonlinear optical interaction can also be a foundation for other down-conversion interactions, including OPG, OPA, as well as OPO.

Sample characterization and experimental setup

In this work, we employ monolayer MoS_2 as a typical representative of TMDs. Monolayer MoS_2 was grown on a SiO_2/Si substrate (the thickness of SiO_2: 285 nm) *via* vapor–liquid–solid method. First, ~2 mg mL^{-1} Na_2MoO_4 aqueous solution was spin-coated on the substrate at 6000 rpm for 30 seconds. Then, the Na_2MoO_4 coating was sulfurized in sulphur vapor to obtain monolayer MoS_2 at 750 °C for 5 min.[29,30] As shown in Fig. 1(a), the MoS_2 flake is typically with a triangle shape. The Raman measurement (Fig. 1(b)) shows peaks of an in-plane mode (E_{2g}) located at ~384 cm^{-1}, and an out-of-plane mode (A_{1g}) at ~402 cm^{-1}. The difference of these two modes is around ~18 cm^{-1}, indicating the monolayer structure. Further, the monolayer MoS_2 flake is characterized by linear optical reflection and photoluminescence measurements. As shown in Fig. 1(c), the three dips at ~421 nm, 604 nm, 650 nm, appear in the reflection spectrum (black curve), corresponding to the C, B, A excitons respectively. In the meantime, the photoluminescence spectrum (red curve) is also plotted in Fig. 1(c). Two photoluminescence peaks (~619 nm and ~673 nm, corresponding to B, A excitons) are obtained by Lorentz fitting, shown as the light- and dark-blue curves. The peak positions are slightly red-shifted comparing with the dips of reflection spectrum, because of large binding energy in the confined structure.[31] The above-mentioned sample characterization experiments indicate that our CVD-grown MoS_2 flakes are typically monolayer with relatively high quality.

Fig. 2(a) shows an illustration of the DFG process in monolayer MoS_2, where a pump photon stimulated by a signal photon, generates two photons at different frequencies (the one with same frequency of signal photon is called signal and the other one is called idler). Therefore, this process typically results in the generation of the idler beam at new wavelengths and the amplification of the incident signal beam. The frequencies of newly generated photons follow the law of energy conservation (*i.e.*, $\omega_{idler}=\omega_{pump}-\omega_{signal}$). The right panel in Fig. 2(a) shows the energy level diagram of DFG.

To perform the DFG interaction, we built an experimental setup as shown in Fig. 2(b). The femtosecond (~150 fs) pulses from an amplified Ti:sapphire laser system at the wavelength of 812 nm with a repetition rate of 2 kHz is employed as the light source. The output beam is first divided into two beams, one is applied for the generation of pump pulses at 406 nm *via* frequency doubling in a BiBO crystal and the other for generating the tunable near-infrared pulses (1300 to 1550 nm) by pumping a TOPAS system (Light conversion). The pump and signal beams are combined by a dichroic mirror (DM) and then focused by an objective (40×, NA. 0.75) on the target sample. The full width at half maximum of the pump and signal beam spots is ~2.5 μm. A delay line is employed in order to synchronize pump and signal pulses. The generated idler is then collected with the same objective lens by a reflection configuration and finally focused into a monochromator followed by a photomultiplier tube (PMT). Colour filters are also used in order to get rid of the residual pump and signal pulses before the monochromator. It should be noted that the repetition rate of our applied laser source (2 kHz) is much

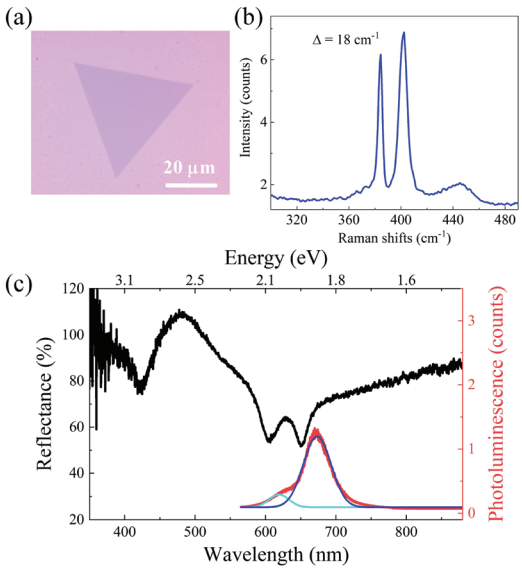

Fig. 1 Optical characterization of monolayer MoS_2. (a) Microscope image, (b) Raman spectrum, where Δ is the difference between two Raman peaks. (c) Linear reflection (black) and photoluminescence (red) spectra. The dark blue and light blue curves are the Lorentz fitting corresponding to the A, B excitonic resonances.

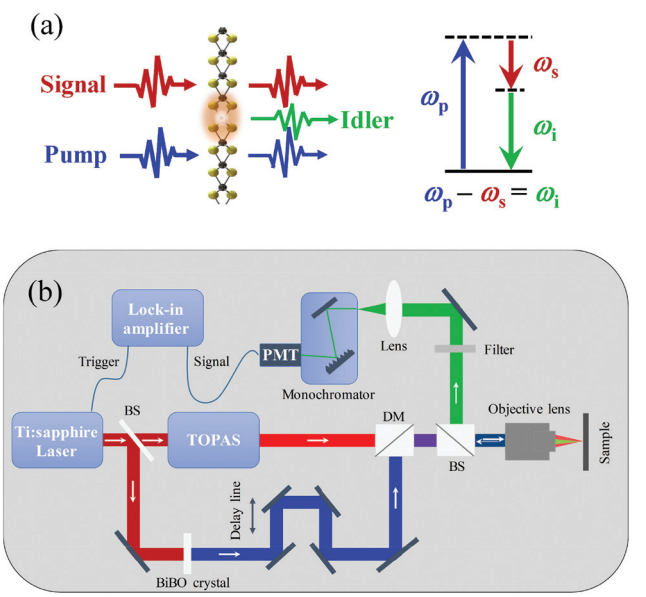

Fig. 2 DFG interaction and experimental setup. (a) An illustration of DFG from monolayer MoS_2; (b) Experimental setup for the DFG interaction. BS: beamsplitter, DM: dichroic mirror, PMT: photomultiplier tube.

lower than the ones (~tens of MHz) typically applied in the previously reported SHG experiments. While such a low repetition rate will not affect the conversion efficiency, it allows advantages including the reduction of the photon-excited luminescence and the thermal effects.

Results and discussion

Fig. 3(a) shows the three-wave mixing spectrum corresponding to the pump pulses with the wavelength of 406 nm and the average power of ~0.9 μW (peak intensity at the focus spot: ~21.18 GW cm^{-2}) and the input signal pulses with the wavelength of 1280 nm and average power of ~3.5 μW (peak intensity at the focus spot: ~82.37 GW cm^{-2}). There are two peaks at wavelengths of ~595 nm and 640 nm, corresponding to the DFG idler and SHG of the signal, respectively. The third peak at 406 nm is the residual pump light after colour filters. The whole spectrum shows the clear evidence of the DFG interaction in monolayer MoS_2. To investigate the DFG at different incident intensities, we measured the power dependence of the output idler as a function of the pump and signal powers. Note that the detected idler power is calibrated with a standard light source. In Fig. 3(b), the power of the generated idler at 595 nm is shown as a function of the pump power, while the signal power is fixed at ~2.5 μW and the pump power is increased from ~0.02 to 0.9 μW. The degradation of sample happens when the pump power is higher than ~0.9 μW. As it is expected from the theoretical formula for the generated DFG idler, the idler power increases linearly, from ~6 to 35 pW. The idler power dependence on the input signal power was measured by increasing the signal power from ~2.5 to 14 μW and fixing the pump power at 0.9 μW as shown in Fig. 3(c). In these conditions, the power of DFG idler also increases linearly with the signal power till 11 μW. However, when the signal power is higher than 11 μW, it becomes saturated which could be attributed to the unbalanced photons of the two input beams. In this regime, the photon number ratio (the signal power of 11 μW and the pump power of 0.9 μW) is about 38 signal photons to 1 pump photon. The participating pump photons are much less than the signal photons at these power levels, limiting the interaction efficiency. Note that all results are repeatable during the measurements.

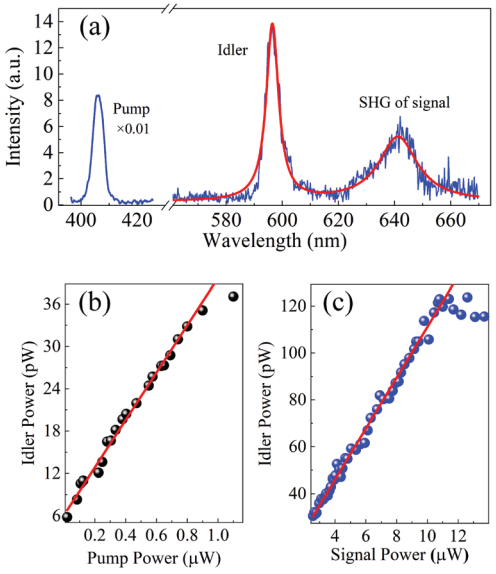

Fig. 3 DFG process in monolayer MoS_2: (a) the generated DFG spectrum; (b) DFG power of the idler at 595 nm as a function of the pump power with the signal power fixed at ~2.5 μW; (c) the DFG idler power dependence on the signal power with the fixed pump power at ~0.9 μW.

In order to estimate the effective second-order nonlinear susceptibility $\chi^{(2)}_{eff}$ of monolayer MoS_2, we simulated the nonlinear optical process in monolayer flake with the coupled-wave equations. Since the thickness of monolayer MoS_2 (L=~0.65 nm) is much smaller than the interacting wavelengths and the DFG is generated within only one layer of molecules, no phase matching consideration is needed. By solving the coupled-wave equations, the $\chi^{(2)}_{eff}$ in the DFG process can be written as[2]

$$\chi^{(2)}_{eff} = \sqrt{\frac{2\varepsilon_0 c^3 I_{si} n_{si} n_{id} n_p}{I_p I_{id} L^2 (\omega_{si})^2}} \quad (1)$$

where ε_0 and c are the permittivity of free space and the speed of light in vacuum, respectively. $n_{id} \cong 4$, $n_{si} \cong 3.6$, and $n_p \cong 3.6$ are the amounts of the refractive indices of the sample at the corresponding idler, signal, and pump wavelengths.[32] I_{id}, I_{si} and I_p are the peak light intensities of the idler, signal and pump pulses, respectively. ω_{si} is the signal frequency.

As shown in Fig. 3(c), the generated idler power at 595 nm can be as high as 120 pW, when the signal power is ~10.5 μW and pump power is ~0.9 μW. This corresponds to a second-order nonlinear susceptibility $\chi^{(2)}_{eff}$ of ~1.8×10^{-8} m V^{-1}, which is comparable to the reported values for MoS_2 in earlier works.[12,14] It should be mentioned that the imperfect temporal and spatial overlaps between the two interacting input pulses in the DFG interaction will notably reduce the interaction efficiency in comparison to the SHG process. In addition, we assume that the substrate introduced doping,[33] strain,[18] and interference[34] effects are to be small in our experiment. In the current condition, the maximum quantum conversion efficiency from the pump to the idler in our DFG process is calculated as ~2×10^{-4}.

We also investigated the relations among polarization directions of the interacting components in the DFG interaction. The structural symmetry group of bulk MoS_2 is D_{6h} with inversion symmetry which leads to zero second-order nonlinearity. While the structural symmetry group of monolayer MoS_2 is D_{3h} with broken inversion symmetry and having strong $\chi^{(2)}$ supporting highly efficient second-order nonlinear optical responses.[13,16] In the $x'y'z'$ crystalline coordinates, the four nonzero elements of $\chi^{(2)}$ tensor for monolayer MoS_2 are $-\chi^{(2)}_{y'x'x'} = \chi^{(2)}_{y'y'y'} = -\chi^{(2)}_{x'y'x'} = -\chi^{(2)}_{x'x'y'}$. In the case of SHG process, the scenario for the polarizations of the interacting beams is simple because of the presence of only one input beam and one output beam as the SHG: the SH radiation components

detected in directions parallel and perpendicular to the polarization of the fundamental field are highly dependent on the azimuthal angle.[13]

Regarding that the DFG interaction is a three-wave interaction: with the pump and signal incident pulses as the input beams and idler as the output, the situation is more complicated and the possible combinations of the relative polarization orientations between each interacting beam and the crystalline axes are increased. In order to check the compatibility of the obtained results with the symmetrical constraints imposed by the D_{3h} symmetry of MoS_2, we performed the analytical calculations for determining the dependence of the generated DFG polarization on the polarization orientations of the input (pump and signal) beams. Supposing the crystal surface in the *xy* plane and the -*z* as the propagation direction of the input pump and signal beams in the lab frame *xyz*, we consider β as the angle between the *x* direction and the crystal armchair direction *x*′, and also α_{id}, α_p and α_{si} as the angles between the idler, pump and signal polarizations, relative to the *x* direction, respectively. After calculating the components of the generated DFG idler in *x*′*y*′*z*′ ($z' = z$) coordinates we will have

$$(E_{id})_{x'} \propto -\sin(2\beta + \alpha_{si} + \alpha_p) \quad (2a)$$

$$(E_{id})_{y'} \propto -\cos(2\beta + \alpha_{si} + \alpha_p) \quad (2b)$$

and after returning to the *xyz* coordinates,

$$(E_{id})_{x} \propto -\sin(3\beta + \alpha_{si} + \alpha_p) \quad (3a)$$

$$(E_{id})_{y} \propto -\cos(3\beta + \alpha_{si} + \alpha_p) \quad (3b)$$

which results in

$$\alpha_{id} = \frac{3\pi}{2} - 3\beta - \alpha_{si} - \alpha_p \quad (4)$$

for the idler polarization angle.

To investigate the generated idler polarization experimentally, we measured the polarization dependence of the generated DFG pulses on the polarization orientations of two input beams. Both the idler and pump polarization orientations were measured relative to the fixed signal polarization which is supposed to be along the *x* direction (α_{si}=0). The angular dependence of the idler power for each pump polarization direction was measured by using a linear polarizer before the detector. The results of such measurement at the pump polarization angle of $\alpha_p = 0°$ are shown in Fig. 4(a) which also confirms the linear polarization of the generated idler pulse. As shown in Fig. 4(b), the linear polarization angles of the idler for different pump polarization orientations are measured. The polarization angles of the idler light (blue dots) show a good agreement with the calculation (eqn (4), red curve). The results confirm the linear dependence of the polarization orientation of the idler beam on the angle between the polarization of each input beam and the crystalline axis *x*′ as demonstrated in eqn (4).

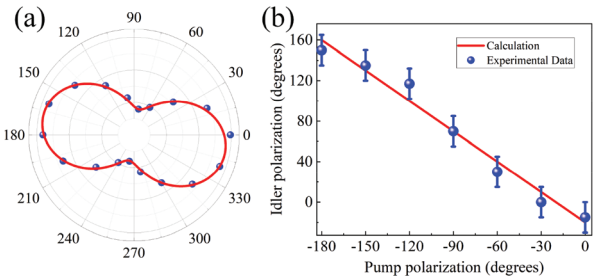

Fig. 4 DFG polarization measurements. (a) Angular dependence of the idler power for fixed pump and signal polarizations at $\alpha_p = \alpha_{si} = 0°$; (b) DFG idler polarization as a function of the pump polarization. The calculated curves (red curves) are the results of analytical determination.

The corresponding behaviour of the MoS_2 monolayers for the DFG at different wavelengths across our available spectral range is also investigated. With the advantage of independence from the limiting phase-matching conditions, in monolayer MoS_2 the nonlinear interactions can be performed across a broad spectral bandwidth. The wavelength of the DFG idler was tuned from 550 to 590 nm by changing the wavelength of signal from 1520 to 1300 nm with the pump wavelength fixed at 406 nm. The experimental data of the generated idler spectra and the Lorentz fitting curves at each wavelength are shown in Fig. 5. The higher generated idler intensities in the spectral region of 570–590 nm could be attributed to the presence of the resonant excitonic effects in this region.[35,36]

Performing the DFG process is a confirmation for the possibility of realizing effective optical parametric interactions. In our experiment, the quantum conversion efficiency is about 2×10^{-4}, which is much higher than that of the most nonlinear responses in monolayer structures. However, because of the practical difficulties, the demonstration of a more efficient OPA process is still far from the reach. In order to improve the conversion efficiency, the exciton enhancement in single-layer TMDs could be employed as an effective solution in the future explorations.[21] While the atomic thickness of monolayer TMDs

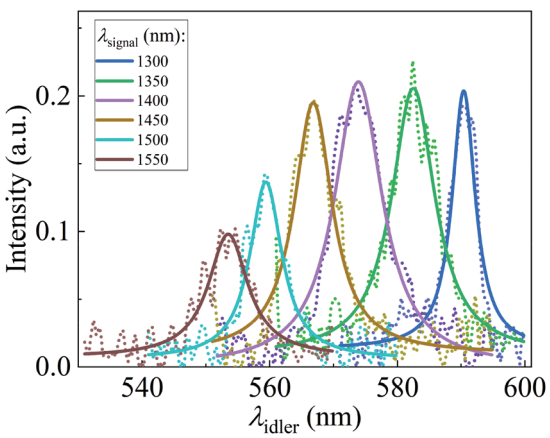

Fig. 5 Tunable DFG at different signal wavelengths with Lorentz fitting.

(~0.65 nm for MoS_2) physically limits the light–matter interaction length, 3R-type bulk MoS_2 with broken inversion symmetry enables strong second-order nonlinear processes, offering a possible method for efficiency improvement.[16,37] On the other hand, integrating monolayer TMDs and other 2D materials with external cavities (such as photonic-crystal nanocavity, microring resonator, whispering-gallery cavity and metallic plasmonics), or waveguides (including microfibers, on-chip waveguides) is also promising for further improvements,[6,38] due to the easy and flexible integration advantages of 2D materials. Furthermore, with assistance of the cavities, OPO operation with 2D materials could be achieved.[39]

Conclusions

We have reported the experimental demonstration of the DFG nonlinear interaction with a second-order nonlinear susceptibility of ~1.8×10^{-8} m V^{-1} in monolayer MoS_2. The generated idler pulses are tunable across the optical spectral range of 550–590 nm by tuning the input signal beam wavelength. The results of this work will pave the way for performing the optical parametric interactions in 2D materials and introducing new tunable light sources in nanoscale.

Conflicts of interest

There are no conflicts to declare.

Acknowledgements

The authors acknowledge the financial support from Aalto Centre for Quantum Engineering, China Scholarship Council (Grant No.: 201606290190), Academy of Finland (Grant No.: 276376, 284548, 295777, 304666, 312297, 312551, and 314810), Academy of Finland Flagship Program (Grant No.: 320167, PREIN), Business Finland (OPEC, A-Photonics), ERC (ATOP), the European Union's Horizon 2020 research and innovation program (Grant No.: 820423, S2QUIP) and the National Natural Science Foundation of China (Grant No.: 11634010, 61775183).

Notes and references

1 Y. R. Shen, *The principles of nonlinear optics*, J. Wiley & Sons, New York, 1984.
2 R. W. Boyd, *Nonlinear Optics*, Academic press, 2007.
3 K. G. Lubic and T. Amano, *J. Chem. Phys.*, 1984, **81**, 1655–1660.
4 D. Richter, A. Fried and P. Weibring, *Laser Photonics Rev.*, 2009, **3**, 343–354.
5 F. Che, S. A. Ponomarenko, M. Cada and N. Nguyen-Huu, *IEEE Photonics J.*, 2017, **9**, 4800511.
6 A. Autere, H. Jussila, Y. Dai, Y. Wang, H. Lipsanen and Z. Sun, *Adv. Mater.*, 2018, **30**, 1705963.
7 Z. Sun, A. Martinez and F. Wang, *Nat. Photonics*, 2016, **10**, 227–238.
8 A. Saynatjoki, L. Karvonen, H. Rostami, A. Autere, S. Mehravar, A. Lombardo, R. A. Norwood, T. Hasan, N. Peyghambarian, H. Lipsanen, K. Kieu, A. C. Ferrari, M. Polini and Z. Sun, *Nat. Commun.*, 2017, **8**, 893.
9 A. Autere, H. Jussila, A. Marini, J. R. M. Saavedra, Y. Dai, A. Säynätjoki, L. Karvonen, H. Yang, B. Amirsolaimani, R. A. Norwood, N. Peyghambarian, H. Lipsanen, K. Kieu, F. J. G. de Abajo and Z. Sun, *Phys. Rev. B: Condens. Matter Mater. Phys.*, 2018, **98**, 115426.
10 H. Liu, Y. Li, Y. S. You, S. Ghimire, T. F. Heinz and D. A. Reis, *Nat. Phys.*, 2016, **13**, 262–265.
11 D. J. Clark, V. Senthilkumar, C. T. Le, D. L. Weerawarne, B. Shim, J. I. Jang, J. H. Shim, J. Cho, Y. Sim, M. J. Seong, S. H. Rhim, A. J. Freeman, K. H. Chung and Y. S. Kim, *Phys. Rev. B: Condens. Matter Mater. Phys.*, 2014, **90**, 121409.
12 L. M. Malard, T. V. Alencar, A. P. M. Barboza, K. F. Mak and A. M. de Paula, *Phys. Rev. B: Condens. Matter Mater. Phys.*, 2013, **87**, 201401.
13 Y. Li, Y. Rao, K. F. Mak, Y. You, S. Wang, C. R. Dean and T. F. Heinz, *Nano Lett.*, 2013, **13**, 3329.
14 N. Kumar, S. Najmaei, Q. Cui, F. Ceballos, P. M. Ajayan, J. Lou and H. Zhao, *Phys. Rev. B: Condens. Matter Mater. Phys.*, 2013, **87**, 161403.
15 X. Yin, Z. Ye, D. A. Chenet, Y. Ye, K. O'Brien, J. C. Hone and X. Zhang, *Science*, 2014, **344**, 488.
16 M. Zhao, Z. Ye, R. Suzuki, Y. Ye, H. Zhu, J. Xiao, Y. Wang, Y. Iwasa and X. Zhang, *Light: Sci. Appl.*, 2016, **5**, 16131.
17 G. Wang, I. C. Gerber, L. Bouet, D. Lagarde, A. Balocchi, M. Vidal, T. Amand, X. Marie and B. Urbaszek, *2D Mater.*, 2015, **2**, 045005.
18 J. Liang, J. Zhang, Z. Li, H. Hong, J. Wang, Z. Zhang, X. Zhou, R. Qiao, J. Xu, P. Gao, Z. Liu, Z. Liu, Z. Sun, S. Meng, K. Liu and D. Yu, *Nano Lett.*, 2017, **17**, 7539–7543.
19 X. Fan, Y. Jiang, X. Zhuang, H. Liu, T. Xu, W. Zheng, P. Fan, H. Li, X. Wu, X. Zhu, Q. Zhang, H. Zhou, W. Hu, X. Wang, L. Sun, X. Duan and A. Pan, *ACS Nano*, 2017, **11**, 4892–4898.
20 X. Lin, Y. Liu, K. Wang, C. Wei, W. Zhang, Y. Yan, Y. J. Li, J. Yao and Y. S. Zhao, *ACS Nano*, 2018, **12**, 689–696.
21 G. Wang, X. Marie, I. Gerber, T. Amand, D. Lagarde, L. Bouet, M. Vidal, A. Balocchi and B. Urbaszek, *Phys. Rev. Lett.*, 2015, **114**, 097403.
22 Y. Song, R. Tian, J. Yang, R. Yin, J. Zhao and X. Gan, *Adv. Opt. Mater.*, 2018, **6**, 1701334.
23 D. Li, W. Xiong, L. Jiang, Z. Xiao, H. R. Golgir, M. Wang, X. Huang, Y. Zhou, Z. Lin, J. Song, S. Ducharme, L. Jiang, J. F. Silvain and Y. Lu, *ACS Nano*, 2016, **10**, 3766–3775.
24 L. Fang, Q. Yuan, H. Fang, X. Gan, J. Li, T. Wang, Q. Zhao, W. Jie and J. Zhao, *Adv. Opt. Mater.*, 2018, **6**, 1800698.
25 K. Yao, E. Yanev, H. J. Chuang, M. R. Rosenberger, X. Xu, T. Darlington, K. M. McCreary, A. T. Hanbicki, K. Watanabe, T. Taniguchi, B. T. Jonker, X. Zhu, D. N. Basov, J. C. Hone and P. J. Schuck, *ACS Nano*, 2020, **14**, 708–714.

26 Y. Zhang, A. Manjavacas, N. J. Hogan, L. Zhou, C. Ayala-Orozco, L. Dong, J. K. Day, P. Nordlander and N. J. Halas, *Nano Lett.*, 2016, **16**, 3373–3378.
27 B. Yao, Y. Liu, S.-W. Huang, C. Choi, Z. Xie, J. F. Flores, Y. Wu, M. Yu, D.-L. Kwong, Y. Huang, Y. Rao, X. Duan and C. W. Wong, *Nat. Photonics*, 2017, **12**, 22–28.
28 T. J. Constant, S. M. Hornett, D. E. Chang and E. Hendry, *Nat. Phys.*, 2015, **12**, 124–127.
29 S. S. Li, Y. C. Lin, W. Zhao, J. Wu, Z. Wang, Z. H. Hu, Y. D. Shen, D. M. Tang, J. Y. Wang, Q. Zhang, H. Zhu, L. Q. Chu, W. J. Zhao, C. Liu, Z. P. Sun, T. Taniguchi, M. Osada, W. Chen, Q. H. Xu, A. T. S. Wee, K. Suenaga, F. Ding and G. Eda, *Nat. Mater.*, 2018, **17**, 535–542.
30 S. S. Li, Y. C. Lin, X. Y. Liu, Z. H. Hu, J. Wu, H. Nakajima, S. Liu, T. Okazaki, W. Chen, T. Minari, Y. Sakuma, K. Tsukagoshi, K. Suenaga, T. Taniguchi and M. Osada, *Nanoscale*, 2019, **11**, 16122–16129.
31 A. Chernikov, T. C. Berkelbach, H. M. Hill, A. Rigosi, Y. Li, O. B. Aslan, D. R. Reichman, M. S. Hybertsen and T. F. Heinz, *Phys. Rev. Lett.*, 2014, **113**, 076802.
32 W. Li, A. G. Birdwell, M. Amani, R. A. Burke, X. Ling, Y.-H. Lee, X. Liang, L. Peng, C. A. Richter, J. Kong, D. J. Gundlach and N. V. Nguyen, *Phys. Rev. B: Condens. Matter Mater. Phys.*, 2014, **90**, 195434.
33 A. Raja, A. Chaves, J. Yu, G. Arefe, H. M. Hill, A. F. Rigosi, T. C. Berkelbach, P. Nagler, C. Schuller, T. Korn, C. Nuckolls, J. Hone, L. E. Brus, T. F. Heinz, D. R. Reichman and A. Chernikov, *Nat. Commun.*, 2017, **8**, 15251.
34 Y. Tang, K. C. Mandal, J. A. McGuire and C. W. Lai, *Phys. Rev. B*, 2016, 94.
35 G. Wang, A. Chernikov, M. M. Glazov, T. F. Heinz, X. Marie, T. Amand and B. Urbaszek, *Rev. Mod. Phys.*, 2018, **90**, 021001.
36 J. Xiao, M. Zhao, Y. Wang and X. Zhang, *Nanophotonics*, 2017, **0**, 1309–1328.
37 J. Shi, P. Yu, F. Liu, P. He, R. Wang, L. Qin, J. Zhou, X. Li, J. Zhou, X. Sui, S. Zhang, Y. Zhang, Q. Zhang, T. C. Sum, X. Qiu, Z. Liu and X. Liu, *Adv. Mater.*, 2017, **29**, 1701486.
38 Z. Sun, *Nat. Photonics*, 2018, **12**, 378–385.
39 A. Ciattoni, A. Marini, C. Rizza and C. Conti, *Light: Sci. Appl.*, 2018, **7**, 5.